Characterisations of the HinOTORI telescope with a three-color imager at Ali Observatory in Western Tibet

W. Liu,[a,b,c,*] **Y. Utsumi,**[d] **Y.Q. Yao,**[e] **K.S. Kawabata,**[b] **M. Sasada,**[b] **M. Yoshida,**[f] **J. Yin**[e] **and Z. Lou**[a,c]

[a] *Purple Mountain Observatory, Chinese Academy of Sciences, Yuanhua Road No.10 Nanjing, China*

[b] *Hiroshima University, 1-4-1 Kagamiyama, Higashi-hiroshima, Hiroshima, Japan*

[c] *Key Laboratory for Radio Astronomy, Chinese Academy of Sciences, Yuanhua Road No.10 Nanjing, China*

[d] *Kavli Institute for Particle Astrophysics and Cosmology, SLAC National Accelerator Laboratory, Stanford University, Menlo Park, California 94025, U.S.A.*

[e] *National Astronomical Observatories of China, Chinese Academy of Sciences, 20A Datun Road Beijing, China*

[f] *Subaru Telescope, National Astronomical Observatory of Japan, 650 North A'ohoku Place, Hilo, Hawaii 96720, U.S.A.*

E-mail: liuwei@pmo.ac.cn

Abstract: HinOTORI is a new telescope supported by an international collaboration project between China and Japan. It is a 50 centimeter telescope equipped with simultaneous three-color imagers (u', R_C, and I_C bands). It is located at Ali Observatory at an altitude of 5100m. Thanks to the high altitude and extreme dryness, Ali site is one of the most suitable sites for optical astrometry. HinOTORI telescope aims at detecting optical transients such as the counterparts of gravitational wave (GW) sources, supernovae, gamma-ray bursts (GRB) and so on. This paper describes the site information, design of simultaneous three-color optical layout, system instruments and whole control system. We also report some telescope characterisations for three bands ($u'/R_C/I_C$) respectively, such as Hartmann constant ($0.49''/0.56''/0.60''$), best focus position (3.922/3.920/3.903 mm), PSF FWHM size (3.755/3.328/3.167pixels), total transmittance and limiting magnitude (15.69/17.57/17.05mag, 10 σ 30 seconds exposure time). With different airmass observation data, the atmospheric extinction coefficients of three bands (0.366/0.061/0.026) were also derived.

Keywords: Control systems; Detectors for UV, visible and IR photons; Optics; Simulation methods and programs

*Corresponding author.

Contents

1 Introduction

Gravitational Waves (GWs) are transverse waves of space strain travelling at the speed of light and were first predicted by Einstein based on his General Relativity. One mechanism to emit GWs is a coalescence of dense compact objects such as black holes and/or neutron stars. GW150914 and GW170817 were two famous events that were caused by two black holes colliding and a binary neutron star coalescence respectively [1–3]. Follow-up observations of these GW events were densely performed by a wide network of global observatories [4].

The early phase of the electromagnetic (EM) emission from a coalescence of binary neutron star system will provide the information of the mechanisms of ejection dynamics and/or nucleosynthesis [5, 6]. Revealing rapid evolution of light curve in different optical band will bring us the information differentiating theoretical models [5, 8]. But it is not easy to identify the localization of GW signals. Advanced LIGO and Advanced Virgo network has demonstrated the ability to localize signals to sky areas of a few tens of square degrees. The addition of KAGRA, and later LIGO-India to the network will improve this situation further. But this is still a challenge for optical telescopes with narrow field-of-view. To search optical counterparts, using a large number of telescopes distributed widely in longitude locations, is a feasible method [7]. The Japanese collaboration for

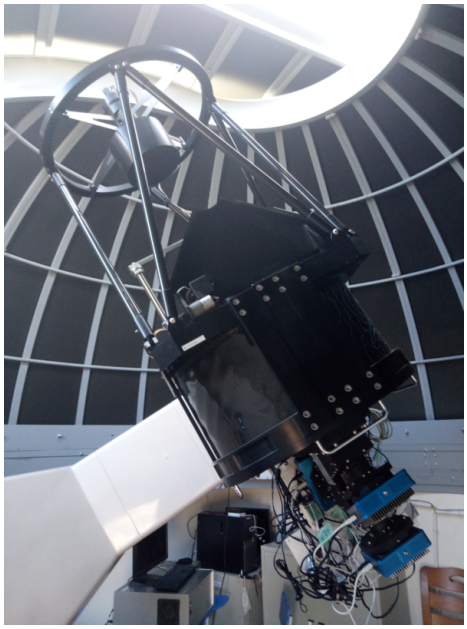

Figure 1. HinOTORI telescope appearance.

Gravitational-wave Electro-Magnetic follow-up (J-GEM) is a telescope network for conducting GW follow-ups. These telescopes are distributed almost all over the world [9–11]. The main tasks of J-GEM include identifying and observing optical counterparts of GW sources in different bands to reveal the physical background of GW sources with multi-message observations. As one member of J-GEM, Hiroshima University Operated Tibet Optical Robotic Imager (HinOTORI) is a 50 cm telescope with three-color (u', R_C and I_C) imagers. Simultaneous photometry in three bands provides accurate information of UV-optical spectral energy distribution and its time variation for GW events. The telescope is located in Ali area at an altitude of 510 0m, in Tibet China, (see figure 1). For most astronomical measurements, observations in the ultraviolet band at wavelengths below 350 nm are not possible from the ground because the light at this band is strongly absorbed by earth's atmosphere, which consists mainly of molecular nitrogen, molecular oxygen, and ozone. At higher altitude, however, the density of atoms and molecules in atmosphere decreases, and the effect of atmospheric absorption is reduced. On the 5100 m altitude site the observation conditions, such as atmospheric transmittance, seeing and sky brightness are more suitable for astronomical observation. In this case, it is feasible for HinOTORI telescope to proceed ultraviolet observations. Moreover HinOTORI can achieve simultaneous three-color imaging with light-weight structure and rapid response. With these advantageous characteristics, HinOTORI can catch up the short-time events, like GW events, transients, supernovae, gamma-ray bursts (GRB) as well as other scientific targets.

2 Site of HinOTORI

Ali site has been developed since 2005 as a potential candidate site for largest class telescopes in the world. The location is at 32° 19′N, 80° 01′E, as high as 5100m above the sea level. It is 30 km away from a nearby town Shiquanhe, with 4300m altitude. Because of its location, HinOTORI can fill the

blank observation zone that J-GEM facilities have not covered. Furthermore, thanks to the high atmospheric transmittance and preferable climate conditions of the site, HinOTORI is also a precious astronomy telescope that can perform scientific observation in UV band on the ground [12]. Early on-site testing efforts revealed some results for conducting astronomical observations. Clearness ratio was 72.3 %, and seeing measured by differential image motion monitor (DIMM) showed a reasonably good observing condition with 0.82 arcsec in 2013 [13].

Recently those efforts were re-evaluated in a more systematic manner and compared to other sites in Feng [14]. From two-year continuous observations data, they showed that the probability of "nights more than 3 hours observable" was 81.71 % and "nights more than 3 hours good observable" was 71.76 %. In terms of sky brightness, the night sky brightness exhibit seasonal change of an order of 1 mag, and the average number of v band is $V = 22\,\mathrm{mag\,arcsec^{-2}}$. Table 1 compares the seeing of Ali and other astronomical sites [14–22].

Table 1. Seeing and brightness for Ali and some of the other high-altitude sites.

Site	Elevation(m)	brightness (mag/arcsec^2)	Seeing ($''$)
La Palma	2344	21.9	0.69
Mauna Kea 13N	4050	21.91	0.75
Hanle	4500	21.28	0.8
Cerro Chajnantor	5640	20.8	0.69
Ali	5100	21.6	0.69

Note: La Palma's seeing was the median value with the ING DIMM on 233 nights. Mauna Kea 13N's seeing value was median value with DIMM from 2005 Jun to 2008 Feb. Hanle's seeing was estimated with DIMM set up in July 1998. The seeing at Cerro Chajnantor was the median value in V-band in 2006–2007. For Ali site,70 % of the sample values were better than 0.9arcsec with DIMM from April to June in 2013. The 50 % of sample values were better than 0.69 arcsec.

3 Design of the HinOTORI system

3.1 Optical design

We developed a wide field simultaneous three-color imaging system for this telescope. The optical system is a classic Ritchey-Chretien system with a primary mirror diameter of 515 mm, focal ratio of f/8 and backfocus of 465 mm. R-C system can eliminate both of spherical and coma aberrations by means of two aspheric mirrors, and two other Seidel aberrations, astigmatism and distortion, remain in the system. To image simultaneously in three band, we used two dichroic mirrors (DM1 and DM2) to split light. Moreover we designed a two-lens corrector system on each channel, inserted wedged glass and determined its wedge angle to minimize the astigmatic aberration of the telescope. For the filters, we installed standard astronomical color filters corresponding to SDSS u' band, Cousins system R_C and I_C band. The central wavelengths of u', R_C and I_C band filters are 348.7 nm, 656.4 nm and 798.0 nm respectively. The filters were placed between the corrector lens system and CCD camera housing. The entire optical layout is shown as figure 2.

3.2 System instruments

The main instruments of the telescope system are listed in table 2.

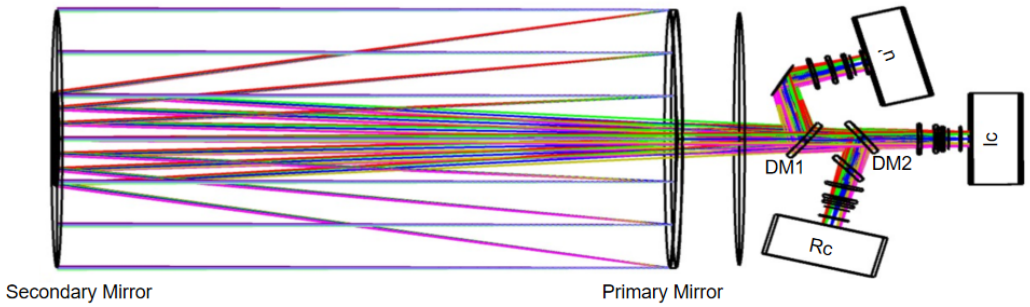

Figure 2. Three-band optical layout.

Table 2. Main instruments list.

Instruments	Manufacture/Model
u' Band Camera	Apogee/Alta F42-UV
R_C and I_C Band Camera	Apogee/Alta F42-MB-HC
Telescope	Alluna Optics/ 515 mm
Mount	Showa /60EL
Dome	Humancom/4-m

We adopted commercial CCD cameras manufactured by Apogee company as the imagers for three bands. For R_C and I_C band, the camera model is Alta F42-MB0F and CCD sensor is back-side illuminated E2VCCD42-40 with 2K × 2K resolution and 13.5 µm square pixels. These two cameras can work at −47°C with two-stage coolers. For u' band, the camera model is Alta F42-UV1F. CCD sensor is the same to the other bands, but Lumogen fluorescence layer was coated on the sensor surface to detect more UV photons. Moreover with its three-stage cooler, u' band camera can work at −57°C, which reduces the dark current significantly. Three bands imagers have the same FoV, which is 24'×24', thus the pixel scale is 0.7arcsec/pixel for all three bands. We employed a custom-made equatorial mount fabricated by SHOWA Inc. To improve the pointing accuracy, an incremental encoder on the right ascension axis was used to enable feedback loop. The maximum slewing speed of mount is 2 degrees/sec.

These telescope instruments are inside a 4-m dome, which was designed by Humancom, Inc., and assembled by HinOTORI team. There is a slit attached to the dome, and the opening and closing actions can be controlled by computerized motors. The dome rotation and slit action are controlled by a synchronizer. It connects to the equatorial mount to read the pointing of telescope with RS232 interface, and can synchronize the dome with telescope pointing. Subsystems such as telescope, mount, dome and cameras can be operated with their respective software. Furthermore, these softwares run under different operating system (Windows and Linux). To integrate software for different systems we employed a virtualization approach to synthesize the cross-system software. The virtualization approach can put all components software on one physical machine. Moreover we employed Internet Communication Engine (ICE) as a middleware to provide the communication among different vendors supplied by software based on different operating systems [23, 24]. Besides these instruments, we deployed rain sensor, UPS, and sky monitor to perform robotical observations.

Liu et al. [25] introduced the HinOTORI telescope control system based on ICE middleware and remote observation system as well.

4 Image quality and focus adjustment

4.1 Hartmann test

We tested the telescope in terms of the image quality using the Hartmann test. The Hartmann test is a convenient way to evaluate image quality of an optical system [26, 28]. At the top of the telescope tube, in front of the secondary mirror, we placed a Hartmann plate that has 20 equally distributed small holes. If the optical system is perfect, the sky starlight passes through these small holes and converges at the focal plane.

Since the aberrations and misalignment cause light to diverge, with Hartmann plate, we took images with CCD shifted forwards and backwards to the ideal focal plane. In this way, intra and extra focus images were obtained, and these images are rotationally symmetrical. We paired 20 spots in the intra-focus image to those in the 180 deg-rotated extra-focus image, then interpolated deviations of 20 spots from the optical axis. Then we analyzed spot diagram to estimate the aberrations. The minimum value of rms of the deviations is Hartmann Constant (HC) and position where the rms value is minimum is defined as the best focus position [27]. In 2018, from the Hartmann test, we calculated HC of u', R_C, and I_C bands were 0.49 ± 0.06, 0.56 ± 0.07 and 0.60 ± 0.07 arcsec, respectively [28].

4.2 Focus adjustment for each channel

We checked the focus position of each camera individually. Each channel has its own dedicated corrector lens system and the cameras themselves have certain tolerance on focus depth. The CCD surface positions from the camera flange were different from each other. Above factors cause focus drift independently. We measured the focus positions of three channels in order to check whether the focus drifts are acceptable. By moving secondary mirror position, focus adjustment can be achieved [28]. The secondary mirror position from its mechanical origin was changed from 3.78 mm to 4.35 mm with the interval of 0.03 mm. We observed the vicinity area of the open cluster NGC 188 ($00^h48^m25.93^s$, $+85°15'18''$) in u', R_C, and I_C bands at 20 different secondary mirror positions. The focus position was shifted back and forth several times. During this process, because of the light-weight structure and small deformations caused by gravity, we think the focus positions were rarely affected by the elevation angle of telescope pointing.

The full-width-at-half-maximums (FWHMs) parameter was used to evaluate the best focus positions with NGC 188 images on different focus positions. Figure 3 is a plot of FWHMs of the observed stellar images versus the secondary mirror positions for three bands.

The relationship between best position and FWHM was identified to obey quadratic function, and we fit those data points with a quadratic function: $\mathrm{FWHM} = a(z - z_{\mathrm{best}})^2 + \mathrm{FWHM}_{\mathrm{min}}$, where the unit of FWHM is pixel scale, and z is secondary mirror position in millimeters. The best fit curves are also shown in figure 3. The best fit parameters and fitting errors are summarized in table 3. The z_{best} of u' band matches well with that of R_C band, but that of I_C band is about 20 µm different from those of the other bands. One possibility is that the distance for I_C band focal surface from the camera flange is not exactly the same as that for the other two bands.

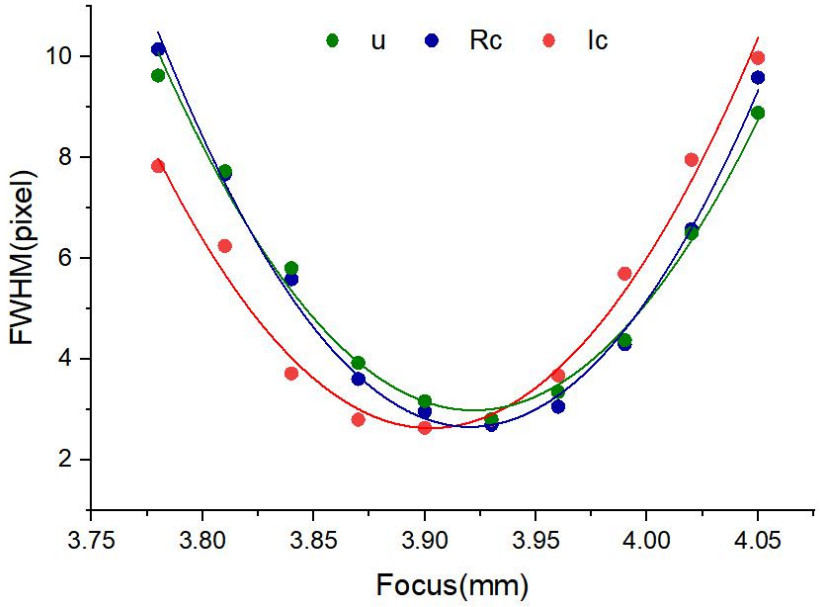

Figure 3. A focus sweep for three bands. The star FWHM is plotted as a function of focus position.

Table 3. The parameters derived from the fitting.

Band	z_{best}	z_{best} error	FWHM_{min}	FWHM_{min} error
u'	3.922	0.002	2.99	0.15
R_{C}	3.920	0.001	2.67	0.13
I_{C}	3.903	0.002	2.64	0.18

4.3 PSF Distribution

Knowing the best focus position, we assessed the image quality across the whole detector area by measuring the point spread function (PSF) parameters. PSF can reflect energy concentration level, and smaller PSF FWHMs lead to deeper limiting magnitudes for point sources. We analyzed the distribution of PSF with SExtractor [29–31], which is a standard image analyzer. It provides measurements of FWHM, ellipticity, magnitude and so on. We observed the region of NGC188 on three bands and analyzed the observation data. NGC188 is an open cluster in the constellation Cepheus, which consists of about 130 stars ranging from 12th to 17th magnitude. By observing this object, there were many stars filling the entire FoV, which can help us to evaluate PSF distribution accurately. The numbers of the standard stars for the flux calibration in u', R_{C}, and I_{C} bands are 7, 596, and 594, respectively. The FWHM and ellipticity distributions are shown as figure 4. For I_{C} band, the average PSF FWHM is 3.167 pixels. The average ellipticity is about 0.133. The average PSF FWHMs/ellipticity for R_{C} and u' bands are 3.328 pixel/0.099 and 3.755 pixels/0.29, respectively. For u' band, the yellow color means that there are no stars in the corresponding fields. Because the number of stars involved in calculation is few, it will cause considerable variation of FWHM and ellipticity. But as a whole, the PSF or ellipticity value follows a uniform distribution, although there are some fluctuations at the edges of focal plane.

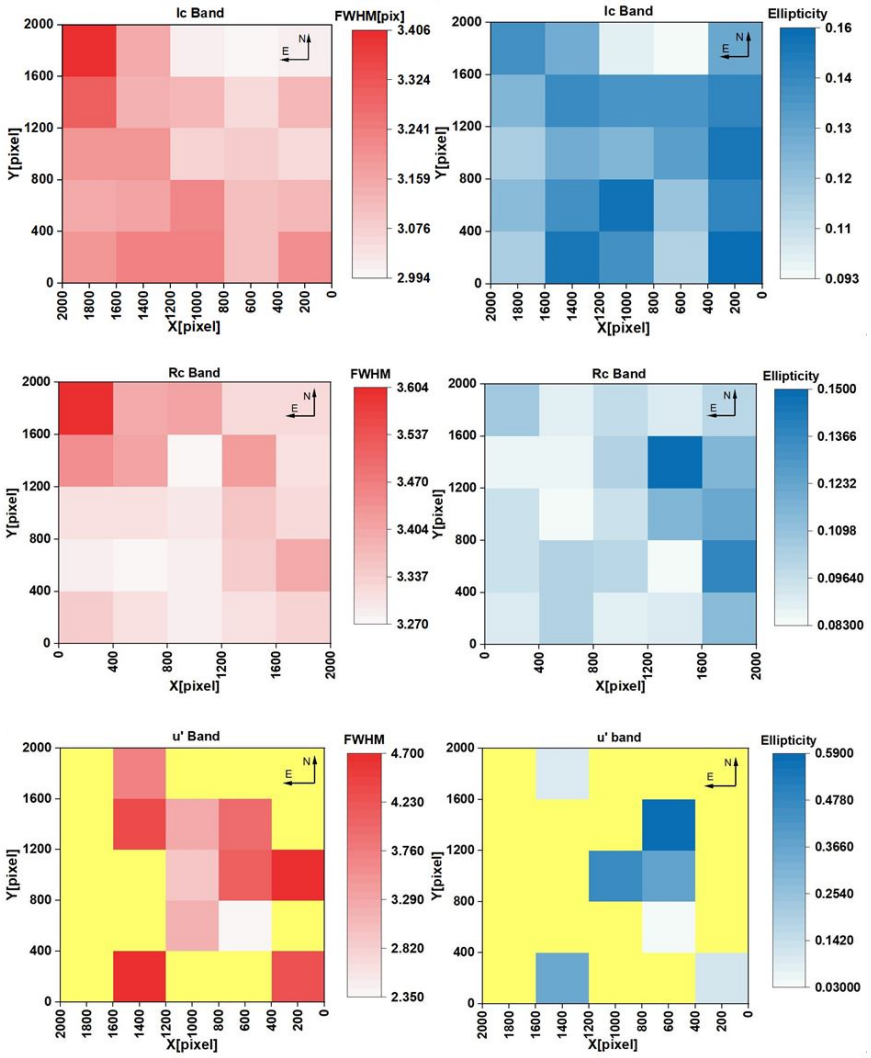

Figure 4. PSF FWHM and ellipticity variation around the focal plane of three bands.

5 System performance

5.1 Total throughput

In section 3.1, we introduced the optical system of the telescope. For optical components in the system, each one has its own throughput and can affect the total transmittance. The component material and coating affect throughput directly. The primary mirror and secondary mirror were made of Al with SiO_2 coating. For calculation of u' band total transmittance, we took primary and secondary mirror coating, one dichroic mirror reflection, planar mirror coating, AR coating of lenses, u' band filter and CCD QE factors into account. With the throughput curve of each factor, we synthesized all factors and plotted the total transmittance as in figure 5. This transmittance is determined by the telescope itself, and atmospheric extinction effect is not included. The total transmittance curves of R_C and I_C bands were synthesized in the same method to the u' band, and the curves are shown in figures 6 and 7.

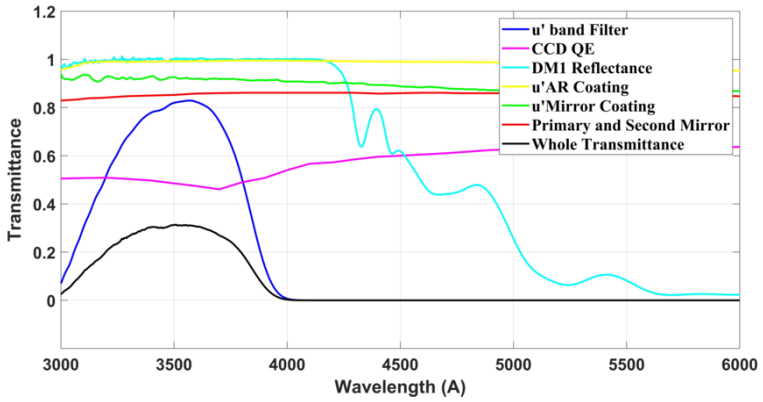

Figure 5. Components and total transmittance of u' band.

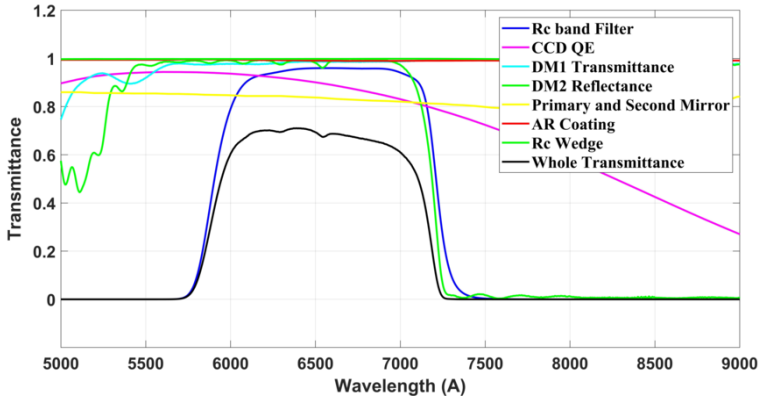

Figure 6. Components and total transmittance of R_C band.

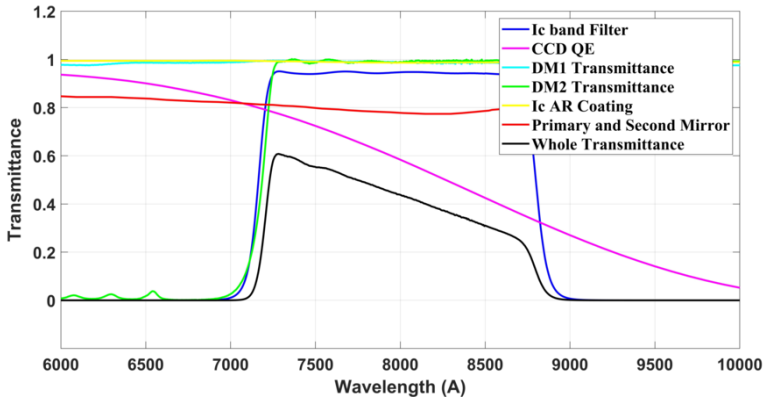

Figure 7. Components and total transmittance of I_C band.

5.2 Atmospheric extinction coefficient

To achieve the absolute photometric measurements on the ground, the atmospheric extinction influence factor should be considered and corrected. The atmospheric extinction coefficient is an important property for a specific astronomical site, and it depends on the density and thickness of atmosphere which radiation passes through. With increasing altitude, the water vapor and aerosol will decrease, and atmosphere thickness and density will reduce, resulting in less influence on the atmospheric extinction. We measured the atmospheric extinction coefficients on high altitude Ali site with images at different zenith angles. At these angles, the instrument magnitude follows this expression.

$$M_{z,\mathrm{band}} = M_{0,\mathrm{band}} + K'_{\mathrm{band}} * F(z) \tag{5.1}$$

Here $M_{z,\mathrm{band}}$ is the apparent magnitude measured inside atmosphere, $M_{0,\mathrm{band}}$ is the extra-atmospheric magnitude, and K'_{band} is atmospheric extinction coefficient. $F(z)$ is airmass which is adopted as follows [32]:

$$\begin{cases} F(z) = \sec z, z \leq 60^\circ \\ F(z) = \sec z - 0.0018167(\sec z - 1) - 0.002875(\sec z - 1)^2 - 0.0008083(\sec z - 1)^3, z > 60^\circ, \end{cases} \tag{5.2}$$

where z is zenith angle in degree. We analyzed three-band images at different zenith angles. From the linear fitting relationship between $(M_{z,\mathrm{band}} - M_{0,\mathrm{band}})$ and $F(z)$, we derived the coefficient K' at $u'/R_{\mathrm{C}}/I_{\mathrm{C}}$ bands. During this process, we observed some UBVRI photometric standard stars whose magnitude are well known. For u' band catalog magnitude, we obtained them from R_{C} and I_{C} band counterparts using the formulas by Jester [33]. For u' band , in consideration of the low atmospheric transmittance, the objects we observed include BD-00 615, HD24401 and TYC 4718-501-1, whose magnitude are about 12 mag, and the exposure time was 240 seconds. The objects adopted for R_{C} and I_{C} bands include BD-00 615, SA95-105 and HD24401, with 10 to 13 magnitudes, and the exposure time was 120 seconds. The airmass changed from 1.6 to 4.5 using equation (5.2) and the fitting results are shown in figure 8. The object offsets on the vertical axis is due to their differences of stellar spectrum. After linear fitting, we got three-band atmospheric extinction coefficients ($\mathrm{K}'_{\mathrm{band}}$) and list them in table 4.

Table 4. Atmospheric extinction coefficient.

Band	K′(mag/airmass)	K′error
u'	0.366	0.005
R_{C}	0.061	0.011
I_{C}	0.026	0.017

5.3 Limiting magnitude

We performed aperture photometry on Nov. 9th 2019. At that time, we took testing images of an open cluster NGC 188 area with 30 seconds exposure time . First, we calibrated zero-point using standard stars. The numbers of standard stars for flux calibration in u', R_{C}, and I_{C} bands are 4, 45, and 45, respectively. By calculating the instrument magnitude and catalog magnitude of

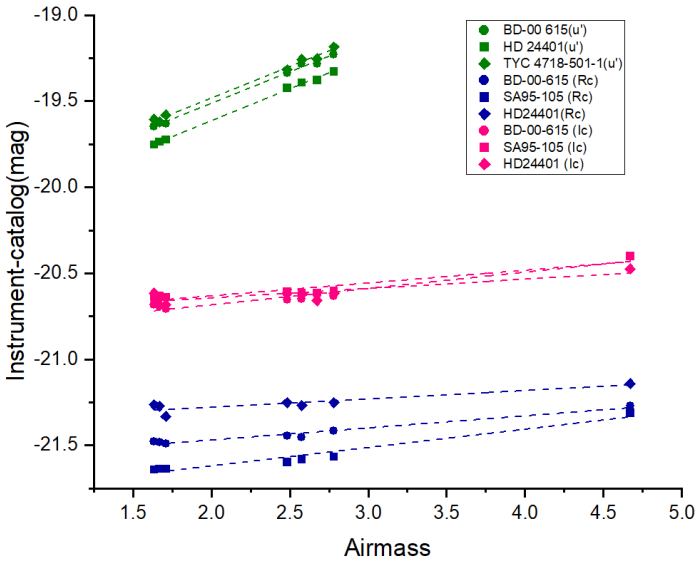

Figure 8. $u'/R_C/I_C$ bands atmospheric extinction coefficient fitting.

standard stars, we obtained ZP values for u', R_C, and I_C bands, which are 24.70 mag, 25.62 mag and 24.77 mag with a 30 sec exposure time, respectively.

The magnitude of an object can be obtained as $M = -2.5\log(\text{count}) + ZP$, where "count" is the observed count value of object in ADU unit. We calculated the signal-to-noise ratio (SNR) using following formula SNR = FLUX_AUTO/FLUXERR_AUTO. The relationship between magnitude error σ_m and SNR is expressed as following formula:[34]

$$\sigma_m = 2.5\log\left(1 + \frac{1}{\text{SNR}}\right) \approx 1.087 \times \frac{1}{\text{SNR}}. \tag{5.3}$$

Figure 9 shows the magnitude versus magnitude error of the photometry. When SNR is equal to 10, the magnitude error will be 0.11. If we take the median value on the error line and all magnitudes are converted to AB magnitude system, the limiting magnitudes of u', R_C, and I_C bands are about 15.69 mag, 17.57 mag, and 17.05 mag respectively, with 30 seconds exposure time for each band. During that observation period, the typical seeing was 1.2 arcsec.

6 Discussion

To evaluate the detectability of the optical emission of the GW source, the ideal case of the limiting magnitudes for HinOTORI telescope are estimated. From the results of 30 second exposure time analysis, it can be speculated that if exposure time in u', R_C, and I_C bands is prolonged to 300s, the limiting magnitude can be 1.25 mag deeper than the calculated value. Furthermore, if seeing is 0.8 arcsec, and aperture size is set to 2 pixels, another 1.56 mag deeper magnitude can be achieved. So the estimation for ideal 10-sigma limiting magnitudes with 300 s exposure time will be 18.50, 20.38 and 19.86 mag corresponding to u', R_C, and I_C bands respectively.

The detectable distance for the GW170817-like source can be estimated from the upper limits of HinOTORI telescope. In the GW170817 light curve scaled by a distance of 100 Mpc, the

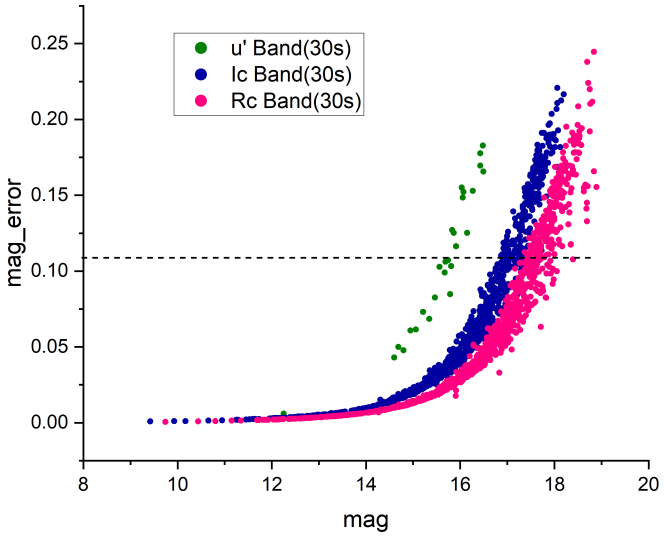

Figure 9. Three bands magnitudes versus magnitude errors aiming at NGC188 area.

peak of apparent magnitude is estimated as $g \sim 19$ mag [6, 7, 11]. The upper limits of the HinOTORI telescope imply a potential to detect the emission at the peak of the GW170817-like object with a distance of 100 Mpc. In the third observing run by Advanced LIGO and Advanced Virgo Collaboration, there are several GW signals which were possibly emitted by binary neutron star (BNS) mergers. GW190425, which was the GW signal from BNS, was located at 159^{+69}_{-72} Mpc. In the nearest case of this event, the optical emission from the source can be detected by HinOTORI telescope. Thus, nearby GW sources within 100 Mpc are good targets to be observed by HinOTORI telescope.

7 Summary and future work

In this paper we presented an overview of HinOTORI telescope, mainly focused on the overall structure, three-color optical design, multi-band CCD cameras, multi-device automatic control method based on ICE communication and so on. For Ali site with 5100 m altitude, the atmospheric extinction coefficients of u', R_C, and I_C bands were measured for the first time and these results are very valuable for other high-altitude projects and telescopes. Now the entire telescope and dome system have been built up, and we can do observation on site or through remote control by network. The observation system now is in the debugging stage, and more accurate parameters will be measured soon afterwards.

As a part of J-GEM, HinOTORI will join the observation of OTs triggered by GWs events, together with Advanced LIGO and Advanced Virgo observing run. Compared to the other telescopes of similar size, HinOTORI has its own advantages including high atmospheric transmittance on high altitude site, simultaneous three-color imaging, highly-automated operation system, etc. These advantages will facilitate the observation of not only GWs, but also gamma-ray burst, supernovae and other variable stars.

Acknowledgments

We thank people living in Ali for their understanding on constructing the astronomical site. We thank the Ali local government for their supports on conducting astronomical research at the valuable location. We thank both of China and Japan governments for their supports on this project. The project was supported by NSFC Grants 11973004.

References

[1] L.-X. Li and B. Paczynski, *Transient events from neutron star mergers*, *Astrophys. J. Lett.* **507** (1998) L59 [astro-ph/9807272].

[2] R. Fernández and B.D. Metzger, *Electromagnetic Signatures of Neutron Star Mergers in the Advanced LIGO Era*, *Ann. Rev. Nucl. Part. Sci.* **66** (2016) 23 [arXiv:1512.05435].

[3] LIGO Scientific, Virgo collaboration, *GW170817: Observation of Gravitational Waves from a Binary Neutron Star Inspiral*, *Phys. Rev. Lett.* **119** (2017) 161101 [arXiv:1710.05832].

[4] LIGO Scientific, Virgo, Fermi-GBM, INTEGRAL collaboration, *Gravitational Waves and Gamma-rays from a Binary Neutron Star Merger: GW170817 and GRB 170817A*, *Astrophys. J. Lett.* **848** (2017) L13 [arXiv:1710.05834].

[5] A.L. Piro and J.A. Kollmeier, *Evidence for Cocoon Emission from the Early Light Curve of SSS17a*, *Astrophys. J.* **855** (2018) 103 [arXiv:1710.05822].

[6] S. Banerjee, M. Tanaka, K. Kawaguchi, D. Kato and G. Gaigalas, *Simulations of early kilonova emission from neutron star mergers*, *Astrophys. J.* **901** (2020) 29 [arXiv:2008.05495].

[7] J-GEM collaboration, *J-GEM optical and near-infrared follow-up of gravitational wave events during LIGO's and Virgo's third observing run*, *PTEP* **2021** (2021) 05A104 arXiv:2106.04842

[8] M. Tanaka et al., *Kilonova from post-merger ejecta as an optical and near-infrared counterpart of GW170817*, *Publ. Astron. Soc. Jap.* **69** (2017) psx12 [arXiv:1710.05850].

[9] T. Morokuma et al., *J-GEM Follow-Up Observations to Search for an Optical Counterpart of The First Gravitational Wave Source GW150914*, *Publ. Astron. Soc. Jap.* **68** (2016) L9 [arXiv:1605.03216].

[10] M. Yoshida et al., *J-GEM follow-up observations of the gravitational wave source GW151226*, *Publ. Astron. Soc. Jap.* **69** (2017) 9 [arXiv:1611.01588].

[11] J-GEM collaboration, *J-GEM observations of an electromagnetic counterpart to the neutron star merger GW170817*, *Publ. Astron. Soc. Jap.* **69** (2017) 101 [arXiv:1710.05848].

[12] P.W.A. Roming et al., *The Swift Ultra-Violet/Optical Telescope*, *Space Sci. Rev.* **120** (2005) 95 [astro-ph/0507413].

[13] Y. Yao, Y. Zhou, L. Liu, H. Wang, J. Yin, X. You et al., *Atmospheric monitoring strategy for the ali site, tibet*, *J. Phys. Conf. Ser.* **595** (2015) 012038.

[14] L. Feng, J.-X. Hao, Z.-H. Cao, J.-M. Bai, J. Yang, X. Zhou et al., *Site testing campaign for the large optical/infrared telescope of china: overview*, *Res. Astron. Astrophys.* **20** (2020) 080.

[15] R.W. Wilson, N. O'Mahony, C. Packham and M. Azzaro, *The seeing at the william herschel telescope*, *Mon. Not. Roy. Astron. Soc.* **309** (1999) 379.

[16] W. Skidmore, S. Els, T. Travouillon, R. Riddle, M. Schöck, E. Bustos et al., *Thirty Meter Telescope Site Testing V: Seeing and Isoplanatic Angle*, *Publ. Astron. Soc. Pac.* **121** (2009) 1151.

[17] R. Cowsik, R. Srinivasan and T.P. Prabhu, *An introduction to the Indian Astronomical Observatory, Hanle*, *Bull. Astron. Soc. India* **30** (2002) 105.

[18] K. M. Motohara, T. Aoki, K. Asano, et al., *Site Characteristics of the Summit of Cerro Chajnantor at the 5640 m Altitude*, *Rev. Mex. Astron. Astrofis. Conf. Ser.* **41** (2011) 83.

[19] L.-Y. Liu, Y.-Q. Yao, J. Vernin, H.-S. Wang, J. Yin and X. Qian, *Multi-instrument characterization of optical turbulence at the ali observatory*, *J. Phys. Conf. Ser.* **595** (2015) 012019.

[20] V.A. Taylor, R.A. Jansen and R.A. Windhorst, *Observing conditions at Mt. Graham: VATT UBVR sky surface brightness and seeing measurements from 1999 through 2003*, *Publ. Astron. Soc. Pac.* **116** (2004) 762 [astro-ph/0406495].

[21] C.S. Stalin, M. Hegde, D.K. Sahu et al., *Night sky at the Indian Astronomical Observatory during 2000–2008*, *Bull. Astron. Soc. India* **36** (2008) 111.

[22] M. Konishi, K. Motohara, K. Tateuchi, H. Takahashi, Y. Kitagawa, N. Kato et al., *ANIR: Atacama near-infrared camera for the 1.0 m miniTAO telescope*, *Publ. Astron. Soc. Jap.* **67** (2015) 4.

[23] Y. Utsumi, S. Kawanomoto, P. Tait, E. Jeschke, H. Furusawa, Y. Kamata et al., *Hyper suprime-cam: the control system*, *Proc. SPIE* **8446** (2012) 844662.

[24] J. Varsik, C. Plymate, P. Goode, A. Kosovichev, W. Cao, R. Coulter et al., *Control and operation of the 1.6 m new solar telescope in big bear*, *Proc. SPIE* **9147** (2014) 91475D.

[25] W. Liu, Y. Utsumi, K.S. Kawabata, M. Sasada, Y. Yao, Y. Zuo et al., *The HinOTORI telescope and its remote control system*, *Proc. SPIE* **11451** (2020) 1145157.

[26] H. Okita, T. Ichikawa, T. Yoshikawa, R.G. Lundock and K. Kurita, *Antarctic infra-red telescope with a 40 cm primary mirror (AIRT40): development and improvement*, *Proc. SPIE* **7733** (2010) 77331U.

[27] H. Ohtani, A. Uesugi, Y. Tomita et al., *The 60 cm Ritchey-Chr´etien telescope and its instruments*, *Mem. Faculty Sci. Univ. Kyoto* **38** (1992) 167.

[28] W. Liu, H. Nagashima, K.S. Kawabata, M. Sasada, Y. Yao and S. Shi, *Best focus approach of HinOTORI telescope*, *Proc. SPIE* **11455** (2020) 114551T.

[29] K. Yanagisawa, Y. Shimizu, K. Okita, D. Kuroda, H. Tsutsui, H. Toda et al., *Okayama astrophysical observatory wide-field camera: status and performance*, *Proc. SPIE* **9908** (2016) 99085D.

[30] S. Noda, J. Furusawa, R. Furusho et al., *PSF analysis of 7 years Subaru/Suprime-Cam data*, *Publ. Nat. Astron. Observ. Jap.* **13** (2010) 71.

[31] H. Zou, T. Zhang, Z. Zhou, J. Nie, X. Peng, X. Zhou et al., *The first data release of the beijing-arizona sky survey*, *Astron. J.* **153** (2017) 276.

[32] H.L. Malasan, D.A. Prabowo, A. Adhyaqsa, M.R. Rabbani, L. Puspitarini and Aprilia, *Study of aerosol content based on spectrophotometric observations: A comparison with long-term extinction profile from photometric observations*, *IOP Conf. Ser. Earth Environ. Sci.* **537** (2020) 012008.

[33] Sloan Digital Sky Survey collaboration, *The SDSS view of the Palomar-Green bright quasar survey*, *Astron. J.* **130** (2005) 873 [astro-ph/0506022].

[34] R. HerBonnet, A. Buddendiek and K. Kuijken, *Shear Nulling after PSF Gaussianisation: moment-based weak lensing measurements with subpercent noise bias*, *Astron. Astrophys.* **599** (2017) A73 [arXiv:1607.02056].